CARBON 63 (2013) 390–396

Available at www.sciencedirect.com

SciVerse ScienceDirect

journal homepage: www.elsevier.com/locate/carbon

Graphene/silver nanowire sandwich structures for transparent conductive films

Bo-Tau Liu *, *Han-Lin Kuo*

Department of Chemical and Materials Engineering, National Yunlin University of Science and Technology, Yunlin 64002, Taiwan

ARTICLE INFO

Article history:
Received 23 April 2013
Accepted 30 June 2013
Available online 4 July 2013

ABSTRACT

We report a simple graphene/silver nanowire (AgNW)/graphene sandwich structure that can be used to prepare highly transparent conductive films; the electrical conductivity of this structure is superior to those of pure AgNW or graphene/AgNW films. Upon increasing the graphene content, the ratio of the direct current (DC) conductivity to the optical conductivity of the three-layer graphene/AgNW/graphene film increased from 4.7 to 44, primarily as a result of connecting and clipping effects. At low contents of AgNW, the graphene played a role of connecting the AgNWs, thereby increasing the DC conductivity by nearly seven orders of magnitude relative to that of pure AgNW films; when the AgNW content was high, the DC conductivity was also enhanced, by 23.8-fold. Observing the second-order zone-boundary phonons, the enhancement in conductivity resulted mainly from tighter contact between the AgNWs, arising from restacking of the top and bottom graphene sheets.

1. Introduction

Transparent conductive films (TCFs) play important roles in such applications as touch panels, liquid crystal displays, solar cells, and organic light emitting diodes. The most commonly used material in the manufacture of TCFs is indium tin oxide (ITO), as a result of its low electrical resistance and high transparency. There are, however, some major problems encountered when applying ITO films, such as their inflexibility and the limited supply of rare metals [1,2]. Over the last two decades, several new materials, including carbon nanotubes [3,4], graphene nanosheets [5], and silver nanowires (AgNWs) [6,7], have been investigated widely as potential replacements for ITO in TCFs. These substitute materials must, however, possess a sheet resistance of less than 100 Ω/sq and a corresponding transmittance greater than 90% in the visible region if they are to meet industry requirements [8,9], In addition, the ratio of the direct current (DC) conductivity to optical conductivity (σ_{DC}/σ_{OP}), a corresponding figure of merit, must be greater than 35; this ratio is determined using the relationship [10,11].

$$\sigma_{DC}/\sigma_{OP} = \frac{Z_0}{2R_s(1/\sqrt{T}-1)} \quad (1)$$

where Z_0 is the impedance of free space (377 Ω) and T and R_s are the transmittance and sheet resistance, respectively. Because of the need for a high value of σ_{DC}/σ_{OP}, carbon nanotubes and AgNWs appear to be the most suitable materials as replacements for ITO in TCFs—especially in resistance-sensitive products, such as solar cells and organic light-emitting diodes [12]. Nevertheless, cost issues currently restrict their applications; it remains a challenge to improve their conductivity and/or decrease their dosages during preparation processes.

The resistance of a carbon nanotube or AgNW film arises mainly at the network junctions of the tubes or wires [13]. Zhu et al. [14] found that TiO_2 sol–gel shrinkage and capillary forces induced by solvent evaporation resulted in tighter

* *Corresponding author:* Fax: +886 5 531 2071.
E-mail address: liubo@yuntech.edu.tw (B.-T. Liu).
0008-6223/$ - see front matter
http://dx.doi.org/10.1016/j.carbon.2013.06.094

contact between crossed AgNWs and, thereby, improved their film conductivity. In addition, Hu et al. [15] reported a simple process for galvanic displacement of a Au coating to decrease wire–wire junction resistance and, thereby, improve conductance. These methods significantly enhance the electrical conductivity of TCFs, providing performances comparable with those of commercial ITO films; they may be less appropriate, however, if the tubes or wires do not intersect or overlap.

Recently, graphene nanosheets have attracted significant attention for their excellent mechanical, optical, thermal, and electrical properties. Most notably, they are cheaper than carbon nanotubes or AgNWs and have an abundant material source, greatly improving their feasibility for practical applications. Unfortunately, graphene has a limitation: its value of σ_{DC}/σ_{OP} is usually less than 10, even when synthesized using chemical vapor deposition [8,16,17]. Some attempts have been made (i) to blend graphene with carbon nanotubes or AgNWs to increase the number of electrically conductive tunnels or lower the percolation limit by virtue of increasing the connectivity between the graphene and the tubes/wires [18–21] and (ii) to dope metal nanoparticles into graphene to increase the connectivity between the nanosheets [22]. Although the results have been very promising, the effects of conductive tunnels or connections are significant only in the low electronic pass routes (few tunnels); the effects may be trivial when the graphene or AgNW content is high. In addition, these methods require the reduction of graphene oxide (GO) to graphene prior to its coating into films; this process usually results in non-uniform films as a result of the difficulty of dispersing reduced GO, which favors restacking, even though doping with metal nanoparticles can have some effect on dispersion [23,24].

In this study, we developed a simple and effective method, combining the contact effect and the connection effect, for the fabrication of TCFs exhibiting improved DC conductivity. By virtue of the connecting and restacking characteristics of graphene, we found that a three-layer graphene/AgNWs/graphene sandwich structure could result in tighter contact of the AgNWs and lower junction resistance. As a result, our graphene/AgNWs/graphene films displayed excellent conductive properties relative to those of pure AgNWs or graphene/AgNW films, potentially minimizing the need for AgNWs and, thus, the cost of TCFs.

2. Experimental

2.1. Materials

Silver nitrate ($AgNO_3$), polyvinylpyrrolidone (PVP), 1,2-aminopropyltriethoxysilane (APTS), and ethylene glycol (EG) were purchased from Sigma–Aldrich. Natural graphite flakes (200 mesh, Alfa Aesar) were used as received. Deionized water (DI water, >18 MΩ cm) was used throughout the experiments.

2.2. Preparation of GO

GO was prepared from natural graphite flakes through a modified Hummers method, as reported elsewhere [25,26], with some of the parameters slightly modified to obtain larger GO sheets. Briefly, graphite flakes (1 g), $NaNO_3$ (1 g), and H_2SO_4 (46 mL, 98%) were mixed in a reaction vessel with an ice-water bath at 0 °C. $KMnO_4$ (6 g) was added slowly to the vessel and then the mixture was stirred continuously at 0 °C for 30 min and then at 40 °C for 3 h. DI water (50 mL) was added slowly to the vessel to dilute the resulting solution. To remove any residual oxidant, H_2O_2 (30%, 5 mL) was added into the mixture, which was then stirred for 10 min. The resulting suspension was washed with DI water through a centrifugation process involving centrifuging the suspension solution, decanting the supernatant, and then redispersing the sediments in water. The process was repeated until the pH reached 7. Finally, the suspension was exfoliated through ultrasonication, resulting in the GO solution.

2.3. Preparation of AgNWs

AgNWs were synthesized using a two-step polyol reduction method [27,28]. 0.3 M PVP (36 mL) and 0.2 M NaCl (80 μL) were mixed in a reaction vessel and heated at 160 °C. 1 M $AgNO_3$ (80 μL) was added into the mixture and then, after 5 min, a further charge of 1 M $AgNO_3$ (4 mL) was added slowly using a peristaltic pump; when the color of the solution turned to a misty auburn, the residual $AgNO_3$ solution was added into the vessel immediately. After 30 min, the as-prepared AgNWs were washed three times with EtOH through centrifugation. As revealed in Fig. 1, the purified AgNWs had lengths of 10–15 μm and diameters of 60–110 nm.

2.4. Preparation of three-layer graphene/AgNWs/graphene TCFs

Glass substrates were washed with EtOH and cleaned using an O_2 plasma cleaner (PDC-23G, Harrick Plasma). The cleaned glass substrates (2.5 × 2.5 cm) were immersed in 10 wt% APTS aqueous solution for 2 min and then intermediately rinsed with DI water and dried at 40 °C. A drop of GO solution (0.1 mg/mL, 50 μL) was placed on an APTS-treated glass substrate, which was then spin-coated (150 rpm, 10 s) and dried (50 °C, 5 min). Different amounts of the AgNW solution (3.5 mg/mL) and the GO solution (0.1 mg/mL) were coated onto the substrates in turn using the same process as mentioned above. No coating solution was spun off the substrate during the spinning process due to the fact that the spin speed is low, the dropped amount is few, and the substrate is highly hydrophilic. Next, the three-layer films were dried at 90 °C for 30 min to enhance their robustness. The films were dipped in 0.3 M $NaBH_4$ solution at room temperature for 30 min and then washed with DI water to remove any residual reductant. Finally, the films were heated at 230 °C for 30 min.

2.5. Characterization

The morphologies of the GO, graphene, AgNWs, and TCFs were examined using optical microscopy (M835, M&T Optics) and field-emission scanning electron microscopy (SEM; S4800-I, Hitachi). Their structures were characterized through X-ray diffraction (XRD) using an X-ray diffractometer

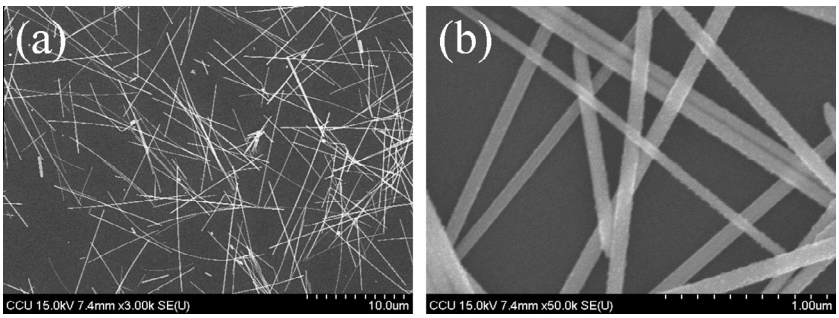

Fig. 1 – Typical SEM images of the as-prepared AgNWs, at various magnifications. (a) ×3 k, (b) ×50 k.

(Miniflex II, Rigaku) and Cu Kα radiation and through micro-Raman spectroscopy using an AFM-Raman system in upright setup (NT-MDT) operating mode at an excitation wavelength of 532 nm. The sheet resistances of the TCFs were determined using a four-pin probe meter (Loresta-GP, Mitsubishi Chemical) with an MCP-T610 probe. The transmittance of each sample was measured at four points using an UV–Vis spectrophotometer (Lambda 850, PerkinElmer).

3. Results and discussion

The as-prepared GO nanosheets, fabricated using a modified Hummers method, had relatively large areas, on the order of hundreds to thousands of square micrometers (Fig. 2a). XRD analysis revealed that the interplanar distance of the (002) planes increased from 0.34 to 0.96 nm after the graphite had been oxidized to GO (Fig. 2b); this result is in good agreement with the findings of previous studies [29,30]. To prepare the three-layer graphene/AgNWs/graphene films, we first fabricated GO/AgNWs/GO three-layer films and then placed them into a solution of a reducing agent to transform the GO to graphene. If we had reduced the first-layer GO (bottom layer) in advance, it became difficult to coat the AgNWs on the surface of the reduced GO, due to low surface energy of graphene. Among the reducing agents commonly employed for the reduction of GO, HI provides the best recovery of the electrical conductivity and the C/O ratio, and is especially good at maintaining integrity and flexibility [31,32]. Unfortunately, HI can react with Ag to form AgI and destroy the nanowire structure. To avoid damaging the AgNWs and reducing the GO in the three-layer structure, we used $NaBH_4$ as a reducing agent for our experiments. The use of $NaBH_4$ for the reduction of GO does, however, have some drawbacks, including the possibility of breaking the films through the production of bubbles and its potential inability to reduce all of the functional groups of GO [33]. We found that the addition of APTS was

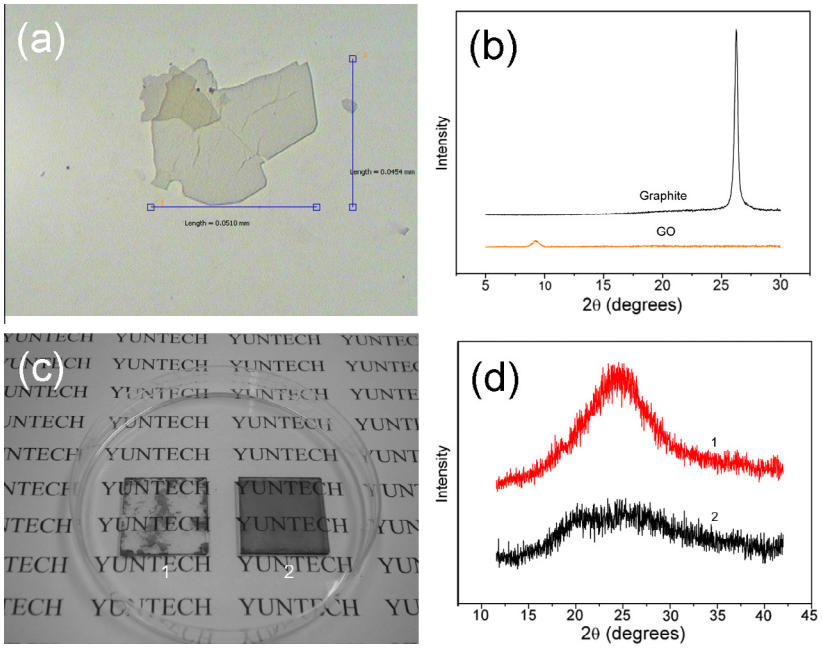

Fig. 2 – (a) Typical optical microscopy image of the as-prepared GO. (b) XRD patterns of graphite and GO; the peak of GO has shifted to a lower angle relative to graphite, indicating that it had exfoliated. (c) Photograph of GO samples reduced by $NaBH_4$ (1) without and (2) with APTS treatment; without APTS treatment, the film was broken down to small debris and peeled off notably, whereas the film with APTS treatment maintained its integrity even when the coating was thick. (d) XRD patterns of reduced GO (1) with and (2) without thermal treatment at 230 °C; the peak intensities have not been rescaled.

helpful to not only to adsorb GO but also to avoid breaking the films down to small debris, thereby maintaining the integrity of the films even at high contents of GO (Fig. 2c). In addition, we found that post thermal annealing of the reduced film provided a higher intensity for the XRD peak representing the restacking of graphene sheets (Fig. 2d), implying that the graphite structure of the film had improved after thermal treatment, thereby enhancing its electrical conductivity. Although a high annealing temperature can assist the recovery of the structure [34], AgNWs may melt or break apart at elevated temperatures; therefore, we chose a thermal treatment temperature of 230 °C for our experiments. Such low-temperature thermal reduction has also been reported in the literature [35,36].

Fig. 3a displays the XRD pattern of the three-layer graphene/AgNWs/graphene film. The dominant peaks had values of 2θ of 37.8 and 44.4°, corresponding to the (111) and (200) planes of Ag, respectively. Although the characteristic peak of graphene overlapped with the pattern of the glass (an inevitability arising from the fact that the three-layer film was transparent), we observed no obvious changes in the locations of the peaks of the three-layer film with respect to those of pristine AgNWs, suggesting that the structures of the AgNWs and graphene were not perturbed during the preparation of the three-layer film. The bright response of the AgNWs in the SEM and optical microscopy images made it difficult to distinguish the top graphene layer in the case of full coverage. Nevertheless, by virtue of the contrast between the covered and uncovered regions (Fig. 3b), we found that the top-layer graphene was patched well on the middle-layer AgNWs. Fig. 4 presents the sheet resistances of the graphene/AgNW hybrid films containing various AgNWs contents. Typically, graphene has conductivity inferior to that of AgNWs. According to the rule of mixtures, the electrical conductivity of a mixture should be between those of its individual components. The addition of graphene, however, significantly improved the conductivity of our graphene/AgNW hybrid films, which displayed conductivities superior to those of pure AgNW films. Moreover, with the same amount of graphene (250 μL), the sheet resistance of a graphene/AgNWs/graphene three-layer structure was much lower than that of a two-layer graphene/AgNWs structure (without the bottom graphene layer). This result implies that a synergetic effect of graphene and AgNWs may occur, depending on the structure and conditions.

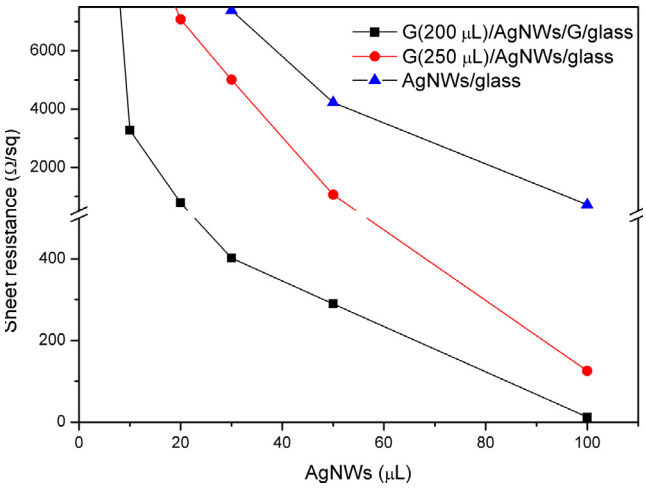

Fig. 4 – Sheet resistances of graphene/AgNW hybrid films having various structures, plotted with respect to the AgNW content.

To further realize the properties of the multilayer hybrid films, we evaluated the effect of the top layer on the conductivity of three-layer graphene/AgNWs/graphene films by varying the amounts of graphene in the top layer. In each case, not surprisingly, we found that the value of σ_{DC}/σ_{OP} of the hybrid films increased upon increasing the content of AgNWs (Fig. 5). The increase was particularly great when the AgNW content was sufficiently high to overcome the percolation threshold. Notably, in the case where we used 100 μL of AgNWs, the value of σ_{DC}/σ_{OP} increased from 4.7 to 44—nearly one order of magnitude—when we increased the amount of graphene used in the top layer from 25 to 200 μL. De and Coleman [8] noted that the value of σ_{DC}/σ_{OP} of graphene prepared from reduced GO in most reports was below 0.7, due to inevitable structural damage caused during rigorous oxidation and exfoliation processes. As a result, we can infer that the enhancement of the value of σ_{DC}/σ_{OP} was not caused by the assistance in electrical conduction arising from the increased content of graphene.

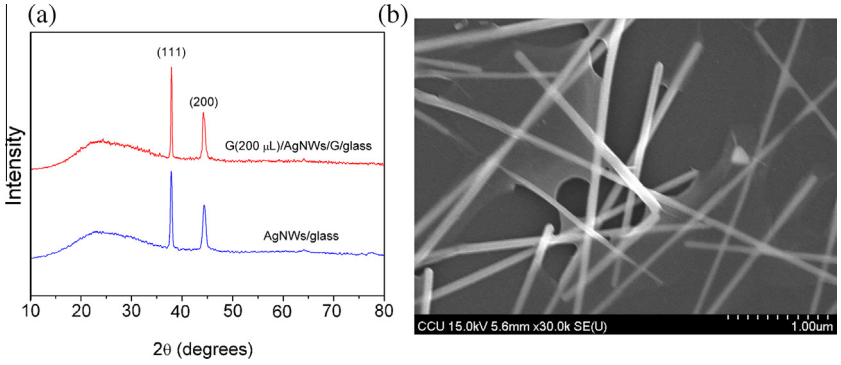

Fig. 3 – (a) XRD patterns of the three-layer graphene/AgNWs/graphene film coated on glass and the as-prepared AgNWs coated on glass. (b) SEM image of the covered and uncovered regions of the three-layer graphene/AgNWs/graphene film, revealing that the top-layer graphene had patched well to the middle-layer AgNWs.

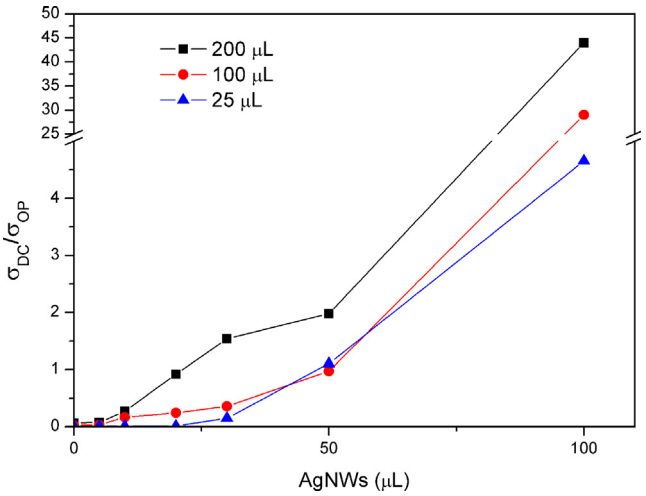

Fig. 5 – Conductivity ratios σ_{DC}/σ_{OP} of three-layer graphene/AgNWs/graphene hybrid films incorporating various amounts of graphene in the top layer, plotted with respect to the AgNW content.

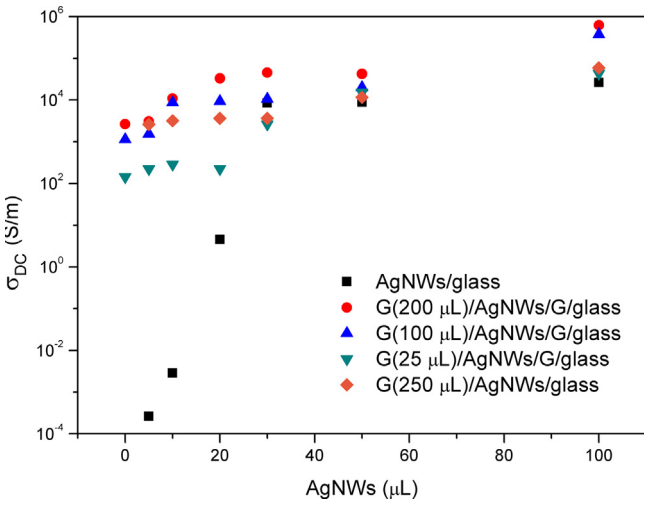

Fig. 6 – DC conductivities (σ_{DC}) of graphene/AgNW hybrid films incorporating various amounts of graphene, plotted with respect to the AgNW content.

The DC conductivity (σ_{DC}) can be regarded as a figure of merit to evaluate the electrical conductive properties of a material. For a thin film, the value can be estimated from

$$\sigma_{DC} = \frac{1}{R_s t} \quad (2)$$

where t is the thickness of the thin film. In this present analysis, we calculated the effective DC conductivities of the graphene layer, the AgNW layer, and their hybrid multilayers using the dense-film approximation (derived from mass balance).

$$t = \frac{\Phi \cdot C}{\rho \cdot A} \quad (3)$$

where Φ is the amount of the coating solution used in the preparation, C is the concentration of the material in the coating solution, ρ is the density of the bulk material, and A is the sample area. We estimated the total thickness of the multilayers from the sum of the thickness of each layer. Fig. 6 provides the values of σ_{DC} for the thin films of various structures. The value of σ_{DC} of the pure AgNW films was very small when the AgNW content was low; it increased upon increasing the AgNW content, ultimately reaching a plateau. In contrast, the DC conductivities of the graphene/AgNW hybrid films were more independent of the AgNW content and typically remained high. As a result, the DC conductivities of the graphene/AgNW hybrid films were significantly higher than those of the pure AgNW films when the AgNW content was low (<30 μL). Nevertheless, the three-layer graphene/AgNWs/graphene films exhibited superior electrical conductivity over the entire range of tested AgNW contents. Comparing the graphene (200 μL)/AgNWs/graphene films with AgNW films, the value of σ_{DC} was 8.6×10^6 times greater for the former when the AgNW content was 5 μL (low AgNW content); moreover, its value remained enhanced, by 23.8-fold, when the AgNW content was 100 μL (high AgNW content).

Fig. 7 displays an AFM scanning image and Raman spectra of the three-layer graphene/AgNWs/graphene films. Because AgNWs are readily destroyed by high-intensity or long-term laser irradiation, we minimized the damaging effects by performing the experiments at room temperature and a low laser power. The Raman spectrum of the pure graphene area (point 1, Fig. 7a) features D (1341 cm^{-1}), Ǵ (1526 cm^{-1}), G (1596 cm^{-1}), 2D (2683 cm^{-1}), and carbonaceous (ca. 2950 cm^{-1}) peaks: the D band is due to the transverse optical phonon branches around the K point, related to defects and structural distortions [37–39]; the Ǵ band is attributed to phonon-induced intraband electronic transitions and appears when graphene is doped [40,41]; the G band is ascribed to the doubly degenerate phonon E_{2g} mode at the Brillouin zone center, corresponding to the graphitic structure [38]; the 2D band corresponds to the second-order zone-boundary phonons, providing information about the electronic structure of the graphene through the double-resonance process [42]; the carbonaceous band arises from CH stretching vibrations [43]. The ratio of the intensities of the G and 2D bands (I_G/I_{2D}) is affected by the thickness of the graphene coating (number of graphene layers) [37,42]. Fig. 7b reveals that the ratio I_G/I_{2D} of the graphene area was larger than that of the three-layer area (point 2, Fig. 7a), suggesting that the top- and bottom-layer graphene may have restacked. In addition, the relative shifts of the G and 2D bands can be used to determine the interactions between the graphene and metal—namely, whether the charge-carrier density or the strain effect dominates. From curves 1 (pure graphene area) and 2 (three-layer area) in Fig. 7b, we observe that the 2D band of the three-layer area had shifted to longer wavelength, whereas the G band was less affected, relative to that of the graphene area. The results suggest that the top-layer graphene suffered from mechanical strain, but did not undergo charge transfer [40,44,45]. Accordingly, we infer that the AgNWs were forced together by the graphene sheets, due to a restacking phenomenon, and that the three-layer structure did not result in electron/hole doping of the graphene.

Fig. 8 depicts a possible mechanism for the enhancement of the electrical conductivity of the graphene/AgNWs/graph-

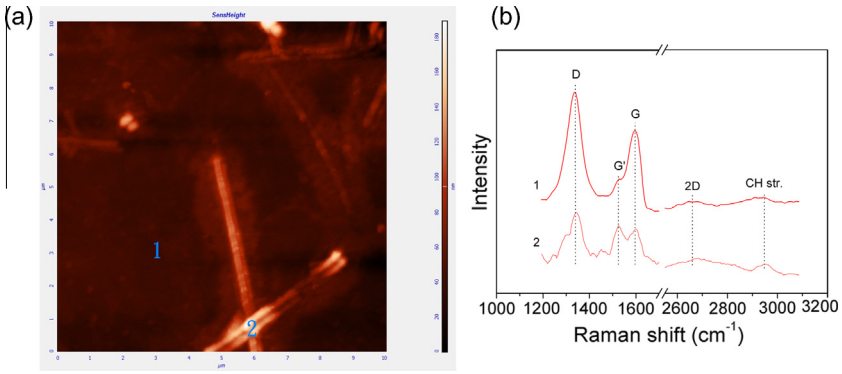

Fig. 7 – (a) AFM image and (b) micro-Raman spectra (measured at 532 nm; (1) graphene area; (2) three-layer area) of the three-layer graphene/AgNWs/graphene hybrid film.

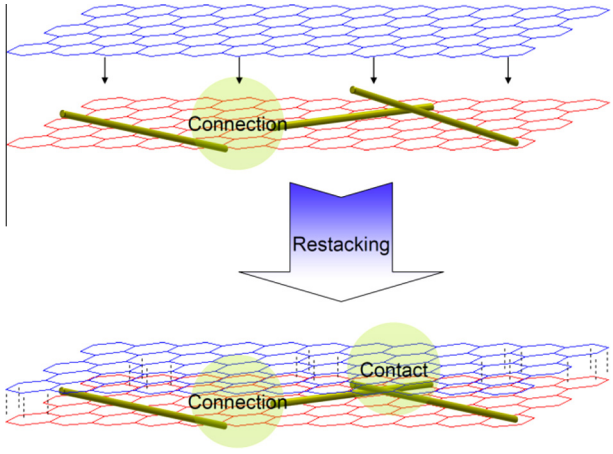

Fig. 8 – Schematic representation of the potential mechanism behind the increased conductivity of the three-layer structure; by virtue of their large areas and restacking characteristics, the graphene nanosheets performed two roles: connecting discrete AgNWs and binding overlapped AgNWs more tightly.

ene thin films. Although its conductivity is inferior to that of AgNWs, we suspect that the graphene played two key roles in affecting the conducting tunnels of the three-layer structure: one as a connector linking discrete AgNWs and the other as a clipper inducing closer contact of overlapped AgNWs. When the AgNW content was low, the connection effect dominated because of the high degree of disconnection among the AgNWs; when the AgNW content was high, however, the contact effect dominated because the main resistance occurred at the junctions of the AgNWs. This mechanism can explain why the two-layer graphene/AgNW films exhibited enhanced DC conductivity at low AgNW contents, but not at high AgNW contents, relative to those of pure AgNW films. Although methods for inducing the tighter contact of AgNWs (using TiO_2 sol–gels or Au coatings) [14,15] and for improving the connection of AgNWs (using graphene) [18,19] have been reported previously in the literature, to the best of our knowledge this present report is the first to describe the synergetic effect of combining the two factors.

4. Conclusion

We have fabricated highly conductive and transparent TCFs incorporating graphene and AgNW layers. The electrical conductivities of our three-layer graphene/AgNWs/graphene films were superior to those of both pure AgNW films and two-layer graphene/AgNWs film. Upon increasing the graphene content, the value of σ_{DC}/σ_{OP} increased from 4.7 to 44, comparable with commercial requirements. With various AgNW contents, the values of σ_{DC} underwent 23.8- to 8.6×10^6-fold enhancements, relative to those of pure AgNW films. In the three-layer structure, the graphene played the role not only of connecting discrete AgNWs but also of binding overlapped AgNWs more tightly by virtue of its restacking characteristics; together, these two factors resulted in the significant enhancements in conductivity.

Acknowledgments

This study was supported financially by the National Science Council of the Republic of China. We thank Professors Mei-Hwa Lee (I-Shou University) and Hung-Yin Lin (National University of Kaohsiung) for their assistance in measurement of the ARM-Raman data.

REFERENCES

[1] Rahy A, Bajaj P, Musselman IH, Hong SH, Sun Y-P, Yang DJ. Coating of carbon nanotubes on flexible substrate and its adhesion study. Appl Surf Sci 2009;255(15):7084–9.
[2] Liu BT, Hsu CH. Anti-scratch and transparency properties of transparent conductive carbon nanotube films improved by incorporating polyethoxysiloxane. J Colloid Interface Sci 2011;359(2):423–7.
[3] Wu Z. Transparent, conductive carbon nanotube films. Science 2004;305(5688):1273–6.
[4] Liu BT, Hsu CH, Wang WH. A comparative study on preparation of conductive and transparent carbon nanotube thin films. J Taiwan Inst Chem Eng 2012;43(1):147–52.
[5] De Arco LG, Zhang Y, Schlenker CW, Ryu K, Thompson ME, Zhou CW. Continuous, highly flexible, and transparent graphene films by chemical vapor deposition for organic photovoltaics. ACS Nano 2010;4(5):2865–73.

[6] Madaria AR, Kumar A, Ishikawa FN, Zhou CW. Uniform, highly conductive, and patterned transparent films of a percolating silver nanowire network on rigid and flexible substrates using a dry transfer technique. Nano Res 2010;3(8):564–73.
[7] Liu CH, Yu X. Silver nanowire-based transparent, flexible, and conductive thin film. Nanoscale Res Lett 2011;6:75.
[8] De S, Coleman JN. Are there fundamental limitations on the sheet resistance and transmittance of thin graphene films? ACS Nano 2010;4(5):2713–20.
[9] Geng HZ, Kim KK, So KP, Lee YS, Chang Y, Lee YH. Effect of acid treatment on carbon nanotube-based flexible transparent conducting films. J Am Chem Soc 2007;129(25):7758–9.
[10] Sorel S, Lyons PE, De S, Dickerson JC, Coleman JN. The dependence of the optoelectrical properties of silver nanowire networks on nanowire length and diameter. Nanotechnology 2012;23(18):185201.
[11] Dressel M, Gruner G. Electrodynamics of solids: Optical properties of electrons in matter. Cambridge: Cambridge University Press; 2002.
[12] Yang LQ, Zhang T, Zhou HX, Price SC, Wiley BJ, You W. Solution-processed flexible polymer solar cells with silver nanowire electrodes. ACS Appl Mater Interfaces 2011;3(10):4075–84.
[13] Nirmalraj PN, Lyons PE, De S, Coleman JN, Boland JJ. Electrical connectivity in single-walled carbon nanotube networks. Nano Lett 2009;9(11):3890–5.
[14] Zhu R, Chung CH, Cha KC, Yang WB, Zheng YB, Zhou HP, et al. Fused silver nanowires with metal oxide nanoparticles and organic polymers for highly transparent conductors. ACS Nano 2011;5(12):9877–82.
[15] Hu LB, Kim HS, Lee JY, Peumans P, Cui Y. Scalable coating and properties of transparent, flexible, silver nanowire electrodes. ACS Nano 2010;4(5):2955–63.
[16] Li XS, Zhu YW, Cai WW, Borysiak M, Han BY, Chen D, et al. Transfer of large-area graphene films for high-performance transparent conductive electrodes. Nano Lett 2009;9(12):4359–63.
[17] Kim J, Ishihara M, Koga Y, Tsugawa K, Hasegawa M, Iijima S. Low-temperature synthesis of large-area graphene-based transparent conductive films using surface wave plasma chemical vapor deposition. Appl Phys Lett 2011;98(9):091502.
[18] Luan VH, Tien HN, Cuong TV, Kong BS, Chung JS, Kim EJ, et al. Novel conductive epoxy composites composed of 2-D chemically reduced graphene and 1-D silver nanowire hybrid fillers. J Mater Chem 2012;22(17):8649–53.
[19] Li CY, Li Z, Zhu HW, Wang KL, Wei JQ, Li XA, et al. Graphene nano-"patches" on a carbon nanotube network for highly transparent/conductive thin film applications. J Phys Chem C 2010;114(33):14008–12.
[20] Yun YS, Kim DH, Kim B, Park HH, Jin HJ. Transparent conducting films based on graphene oxide/silver nanowire hybrids with high flexibility. Synth Met 2012;162(15–16):1364–8.
[21] Liu Y, Chang Q, Huang L. Transparent, flexible conducting graphene hybrid films with a subpercolating network of silver nanowires. J Mater Chem C 2013;1(17):2970–4.
[22] Tien HW, Huang YL, Yang SY, Wang JY, Ma CCM. The production of graphene nanosheets decorated with silver nanoparticles for use in transparent, conductive films. Carbon 2011;49(5):1550–60.
[23] Tang XZ, Cao ZW, Zhang HB, Liu J, Yu ZZ. Growth of silver nanocrystals on graphene by simultaneous reduction of graphene oxide and silver ions with a rapid and efficient one-step approach. Chem Commun 2011;47(11):3084–6.
[24] Xu C, Wang X, Zhu JW. Graphene-metal particle nanocomposites. J Phys Chem C 2008;112(50):19841–5.
[25] Hummers WS, Offeman RE. Preparation of graphitic oxide. J Am Chem Soc 1958;80(6):1339.
[26] Marcano DC, Kosynkin DV, Berlin JM, Sinitskii A, Sun ZZ, Slesarev A, et al. Improved synthesis of graphene oxide. ACS Nano 2010;4(8):4806–14.
[27] Hu MJ, Gao JF, Dong YC, Li K, Shan GC, Yang SL, et al. Flexible transparent PES/silver nanowires/PET sandwich-structured film for high-efficiency electromagnetic interference shielding. Langmuir 2012;28(18):7101–6.
[28] Hu MJ, Gao JF, Dong YC, Yang SL, Li RKY. Rapid controllable high-concentration synthesis and mutual attachment of silver nanowires. RSC Adv 2012;2(5):2055–60.
[29] Schniepp HC, Li JL, McAllister MJ, Sai H, Herrera-Alonso M, Adamson DH, et al. Functionalized single graphene sheets derived from splitting graphite oxide. J Phys Chem B 2006;110(17):8535–9.
[30] Fan ZJ, Kai W, Yan J, Wei T, Zhi LJ, Feng J, et al. Facile synthesis of graphene nanosheets via Fe reduction of exfoliated graphite oxide. ACS Nano 2011;5(1):191–8.
[31] Pei SF, Zhao JP, Du JH, Ren WC, Cheng HM. Direct reduction of graphene oxide films into highly conductive and flexible graphene films by hydrohalic acids. Carbon 2010;48(15):4466–74.
[32] Zhao JP, Pei SF, Ren WC, Gao LB, Cheng HM. Efficient preparation of large-area graphene oxide sheets for transparent conductive films. ACS Nano 2010;4(9):5245–52.
[33] Langley LA, Fairbrother DH. Effect of wet chemical treatments on the distribution of surface oxides on carbonaceous materials. Carbon 2007;45(1):47–54.
[34] Geng JX, Liu LJ, Yang SB, Youn SC, Kim DW, Lee JS, et al. A simple approach for preparing transparent conductive graphene films using the controlled chemical reduction of exfoliated graphene oxide in an aqueous suspension. J Phys Chem C 2010;114(34):14433–40.
[35] Yang L, Kong J, Yee WA, Liu W, Phua SL, Toh CL, et al. Highly conductive graphene by low-temperature thermal reduction and in situ preparation of conductive polymer nanocomposites. Nanoscale 2012;4(16):4968–71.
[36] Yang SJ, Kim T, Jung H, Park CR. The effect of heating rate on porosity production during the low temperature reduction of graphite oxide. Carbon 2013;53:73–80.
[37] Entani S, Sakai S, Matsumoto Y, Naramoto H, Hao T, Maeda Y. Interface properties of metal/graphene heterostructures studied by micro-Raman spectroscopy. J Phys Chem C 2010;114(47):20042–8.
[38] Tuinstra F, Koenig JL. Raman spectrum of graphite. J Chem Phys 1970;53(3):1126–30.
[39] Ferrari AC, Robertson J. Interpretation of Raman spectra of disordered and amorphous carbon. Phys Rev B 2000;61(20):14095–107.
[40] Wang WX, Liang SH, Yu T, Li DH, Li YB, Han XF. The study of interaction between graphene and metals by Raman spectroscopy. J Appl Phys 2011;109(7):07C501.
[41] Hulman M, Haluska M, Scalia G, Obergfell D, Roth S. Effects of charge impurities and laser energy on Raman spectra of graphene. Nano Lett 2008;8(11):3594–7.
[42] Ferrari AC, Meyer JC, Scardaci V, Casiraghi C, Lazzeri M, Mauri F, et al. Raman spectrum of graphene and graphene layers. Phys Rev Lett 2006;97(18):187401.
[43] Stadler J, Schmid T, Zenobi R. Nanoscale chemical imaging of single-layer graphene. ACS Nano 2011;5(10):8442–8.
[44] Stampfer C, Molitor F, Graf D, Ensslin K, Jungen A, Hierold C, et al. Raman imaging of doping domains in graphene on SiO_2. Appl Phys Lett 2007;91(24):241907.
[45] Das A, Pisana S, Chakraborty B, Piscanec S, Saha SK, Waghmare UV, et al. Monitoring dopants by Raman scattering in an electrochemically top-gated graphene transistor. Nat Nanotechnol 2008;3(4):210–5.